A Robust Timing Synchronization Design in OFDM Systems–Part I: Low-Mobility Cases

Yasamin Mostofi, *Member, IEEE* and Donald C. Cox, *Fellow, IEEE*

***Abstract*— In this paper we are interested in designing a robust timing synchronization algorithm for OFDM systems that utilize pilot-aided channel estimation. We first characterize the impact of timing errors on the performance of a pilot-aided OFDM system. We derive analytical expressions for average channel estimation error variance in the presence of timing errors in high delay spread fading environments. The derived expressions show that pilot-aided channel estimators are considerably sensitive to timing synchronization errors due to the impact of rotations in different bases. We then show how to utilize this sensitivity to design a robust timing synchronization algorithm, *without* training overhead. The proposed algorithm is a cross-block design that uses channel estimation information to improve timing synchronization. We confirm our analytical results by simulating the proposed algorithm in high delay spread fading environments. In this paper, i.e. Part I, we focus on timing synchronization for low-mobility cases. The analysis and results are then extended to high-mobility applications in Part II.**

***Index Terms*— Channel estimation, orthogonal frequency division multiplexing (OFDM), timing synchronization.**

I. Introduction

THERE has recently been considerable interest in Orthogonal Frequency Division Multiplexing (OFDM) systems. In OFDM systems the given bandwidth is divided into narrow sub-channels. By transmitting low data rates in parallel on these sub-channels, OFDM systems can handle high delay spread environments [4], [20], [21]. By adding a guard interval to the beginning of each OFDM symbol, the effect of delay spread (provided that there is perfect synchronization) would appear as a multiplication in the frequency domain for a time-invariant channel. This feature allows for higher data rates and has resulted in the selection of OFDM as a standard for Digital Audio Broadcasting (DAB [5]), Digital Video Broadcasting (DVB [16]), and wireless local area networks (802.11a).

The performance of OFDM systems, however, is sensitive to the performance of the timing synchronizer. Timing synchronization, in this paper, refers to the correct detection of the start of an OFDM symbol. Timing synchronization errors degrade the performance of an OFDM receiver by introducing Inter-Carrier-Interference (ICI) and Inter-OFDM Symbol-Interference (ISI). Research in timing synchronization of OFDM systems has mainly focused on fixed wireless applications and can be primarily categorized into two main groups: training-based and correlation-based. The first group is based on transmitting training information for synchronization [3], [10], [11], [12], [17]. Muller et al. has provided a good survey and comparison of such algorithms [12]. In these algorithms, there is a waste of bandwidth in transmitting the training data. In the algorithm proposed by Schmidl et al. [17], half of the subcarriers are occupied by known information for timing synchronization. This inserted frequency-domain training information results in repetition in time domain, which is then exploited for timing synchronization in the receiver. Similarly, Minn et al. [10] proposes a synchronization algorithm in the same category as Schmidl et al., i.e. based on using training information. Essentially, in their case, most of the subcarriers are devoted for transmitting training information. They further do limited performance improvement by estimating the delay of the first channel path.

The second category is based on using the redundancy of the cyclic prefix [6], [19]. Then the start of the symbol is where the correlation of the start and end data points is maximized. In the absence of delay spread, this would work fine. However, in the presence of delay spread, the cyclic prefix would be affected by the previous OFDM symbol resulting in performance degradation. There are also blind algorithms that attempt to perform timing synchronization by using cylcostationary properties, without relying on the cyclic prefix or training information [2], [14]. The processing delay and computational complexity of these algorithms, however, can be high, making it unfeasible for high delay and Doppler spread environments.

There are other methods that use cyclic prefix for coarse synchronization followed by a fine tuning based on an impact on channel estimation [22], [18]. These algorithms are more in the same category as ours in the sense that they do not rely on training information. Yang et al. [22] uses the pilots inserted for channel estimation to perform coarse timing synchronization. They fine tune their algorithm by trying to estimate the delay of the first channel path. In doing so, they assume that the first channel path is the strongest, which may not be the case. Furthermore, they need to do averaging over a number of OFDM symbols, which increases the delay. In our case we are interested in timing synchronization by using the information of only one OFDM symbol. Furthermore, we are interested in synchronization in the presence of channels that do not necessarily have the first path the strongest. Speth et al. [18] proposed using the redundancy of the cyclic prefix for coarse synchronization followed by fine tuning the performance by

Manuscript received May 1, 2006; revised December 19, 2006; accepted May 30, 2007. The associate editor coordinating the review of this paper and approving it for publication was C. Tellambura.

Y. Mostofi is with the Department of Electrical and Computer Engineering, University of New Mexico, Albuquerque, NM, 87131 USA (e-mail: ymostofi@ece.unm.edu).

D. C. Cox is with the Department of Electrical Engineering, Stanford University, Stanford, CA, 94305 USA (e-mail: dcox@spark.stanford.edu).

Digital Object Identifier 10.1109/TWC.2007.xxxxx.

minimizing the following metric: $\sum_{l\in pilots}|z_l - p_l\tilde{H}(l)|^2$, where z_l denotes the frequency domain l^{th} received sample, p_l is the pilot at l^{th} subcarrier and $\tilde{H}(l)$ is the estimated channel at l^{th} subcarrier.

In this paper we take a different approach. We are interested in designing a robust timing synchronizer that does not rely on synchronization training information, for pilot-aided OFDM systems in high delay spread environments. We first analyze the impact of timing synchronization errors on the performance of a pilot-aided channel estimator by deriving an analytical expression for channel estimation error variance in the presence of timing errors and for a frequency-selective fading channel. We find that for a pilot-aided channel esitmator, the equivalent channel and the estimated equivalent channel have rotations in different bases. Our mathematical derivations will show that, due to this effect, a pilot-aided channel estimator is considerably sensitive to timing synchronization errors. We then show how to utilize this sensitivity to design a robust timing synchronization algorithm, *without* training overhead. The proposed algorithm is a cross-block design that uses channel estimation information to improve timing synchronization. In this paper, i.e. Part I, we focus on timing synchronization in low-mobility environments, where channel can be taken constant over one OFDM symbol. The analysis and results are then extended to high-mobility applications in Part II.

We conclude this section with an overview of the paper. In Section II we summarize system model of an OFDM system that utilizes pilot-aided channel estimation assuming perfect synchronization. After briefly reviewing the impact of timing synchronization errors on an OFDM system in Section III, we derive analytical expressions for average channel estimation error variance of a pilot-aided channel estimator in the presence of timing errors in Section IV. The results of Section IV show the super-sensitivity of a pilot-aided channel estimator to timing synchronization errors. In Section V, we then show how to utilize this sensitivity to design a timing synchronization algorithm that works robustly even in considerably high delay spread fading environments such as those experienced in Single Frequency Networks (SFN). Section VI shows the performance of the proposed synchronizer in high delay spread fading environments. It also provides a comparison with other existing algorithms. Section VII summarizes the results and briefly discusses possible future extensions.

II. Ideal Case: Perfect Synchronization

In this section we summarize the system model of an OFDM system that utilizes a pilot-aided channel estimator assuming perfect synchronization.

A. System Model

Consider an OFDM system in which the available bandwidth is divided into N sub-channels and the guard interval spans G sampling periods. X_i represents the transmitted data point in the i^{th} frequency sub-band and is related to the time domain sequence, x_k, as follows:

$$X_i = \sum_{k=0}^{N-1} x_k e^{-\frac{j2\pi ki}{N}} \quad 0 \le i \le N-1. \tag{1}$$

$\vec{x}_{pf}$ is the cyclic prefix vector with length G and is related to x as follows:

$$\vec{x}_{pf}(i) = x_{N-G+i} \quad 0 \le i \le G-1. \tag{2}$$

Let T represent the length of one OFDM symbol after adding the guard interval. Then $T_s = \frac{T}{N+G}$ represents the sampling period. We assume that the normalized length of the channel delay spread (normalized to the sampling period) is always less than or equal to G. Let h_k represent the k^{th} channel path. h_k has Rayleigh fading amplitude and uniformly distributed phase. In this paper, we take the channel to be constant over one OFDM symbol and leave the case of high mobility OFDM to Part II. Let y_i represent i^{th} sample of the channel output. We will have:

$$y_i = \overbrace{\sum_{k=0}^{G} h_k x_{((i-k))_N}}^{\vartheta_i} + w_i \quad 0 \le i \le N-1, \tag{3}$$

where $((\quad))_N$ represents a cyclic shift in the base of N and w_i represents a sample of additive white Gaussian noise. Then Y, the FFT of sequence y, will be as follows:

$$Y_i = H_i X_i + W_i \quad 0 \le i \le N-1, \tag{4}$$

where H and W denote the FFTs of the sequences h and w. To retrieve the transmitted data points from Eq. 4, the gain and phase of the channel should be estimated. In this paper, we use frequency-domain pilot tones for channel estimation.

B. Pilot-Aided Channel Estimation

Let $\nu \le G$ represent the maximum predicted normalized length of the channel delay spread. Therefore, only $L = \nu + 1$ equally-spaced pilot tones, $X_{pilot}(l_i)$ for $0 \le i \le L-1$, are needed to estimate channel frequency response [13], where $l_i = \frac{i\times N}{L}$. Then,

$$\hat{H}_{l_i} = \frac{Y_{l_i}}{X_{pilot}(l_i)} = H_{l_i} + \frac{W_{l_i}}{X_{pilot}(l_i)} \quad 0 \le i \le L-1, \tag{5}$$

where $\hat{H}_{l_i}$ is the estimate of the channel at the l_ith sub-carrier. Through an IFFT of length L, the estimate of the channel in time domain would be

$$\hat{h}_k = \frac{1}{L}\sum_{i=0}^{L-1} \hat{H}_{l_i} e^{\frac{j2\pi ik}{L}} \quad 0 \le k \le L-1. \tag{6}$$

Then through an FFT of length N, the estimate of the channel at all the sub-carriers will be

$$\hat{H}_i = \sum_{k=0}^{L-1} \hat{h}_k e^{-\frac{j2\pi ik}{N}} \quad 0 \le i \le N-1. \tag{7}$$

Equivalent of these operations can also be characterized as a frequency-domain interpolation. See [9] for details.

III. Effect of Timing Synchronization Errors

In this paper, we take the timing error to be a multiple of the sampling period to ease mathematical derivations. The analysis and results can be extended to the sub-sample level using the models developed in [8]. Consider a case of a timing error of m sampling periods. In this paper, $m > 0$ and $m < 0$ denote timing errors of m to the right and left sides respectively. We assume that $|m| < L$ (or equivalently $|m| < G$ since G and L are both chosen based on the maximum predicted channel length) in this paper. In this section, we will characterize the impact of timing synchronization errors on an OFDM system.

A. Case of Timing Errors to the Right $(m > 0)$

In this case an error of m sampling periods to the right side has occurred. Then, the terms $y_0, y_1, \ldots, y_{m-1}$ are missed and instead m data points of the next OFDM symbol are erroneously selected. The received signal can thus be written as follows:

$$y_i^r = \vartheta_{((i+m))_N} \times \gamma_i^r + s_i + w_i^r \quad 0 \le i \le N-1, \tag{8}$$

where y_i^r is i^{th} sample of the received signal for $m > 0$, ϑ is as defined in Eq. 3, w_i^r is a sample of AWGN, $s_i = \begin{cases} 0 & 0 \le i \le N-m-1 \\ y_{pf}^{next}(i-N+m) & else \end{cases}$ and $\gamma_i^r = \begin{cases} 1 & 0 \le i \le N-m-1 \\ 0 & N-m \le i \le N-1 \end{cases} \cdot\, y_{pf}^{next}(i)$ for $0 \le i \le m-1$ represents the i^{th} sample of the output cyclic prefix of the next OFDM symbol (excluding the effect of AWGN):

$$y_{pf}^{next}(i) = \overbrace{\sum_{k'=i+1}^{C} h_{k'} x_{N-k'+i}}^{\text{ICI}} + \overbrace{\sum_{k'=0}^{i} h_{k'} x_{N-G+i-k'}^{next}}^{\text{ISI}}, \tag{9}$$

where $C \le \nu$ represents the normalized length of the channel delay spread and x^{next} denotes the time-domain transmitted data of the next OFDM symbol. Then Y_i^r, the FFT of y_i^r, will be as follows for $0 \le i \le N-1$,

$$\begin{aligned} Y_i^r &= \frac{\Gamma_0^r}{N} H_i X_i e^{\frac{j2\pi mi}{N}} \\ &+ \underbrace{\overbrace{\sum_{k=1}^{N-1} \frac{\Gamma_k^r}{N} H_{((i-k))_N} X_{((i-k))_N} e^{\frac{j2\pi m(i-k)}{N}}}^{I_i^r} + S_i + W_i^r}_{\text{ICI \& ISI}} \end{aligned} \tag{10}$$

Where S_i is the FFT of s_i and Γ_i^r, the FFT of γ_i^r, is $\Gamma_i^r = \begin{cases} \frac{1-e^{j2\pi im}}{1-e^{-\frac{j2\pi i}{N}}} & i \ne 0 \\ N-m & i = 0 \end{cases}$. Then $\overline{|I_i^r + S_i|^2}$ represents the average interference power, including both ICI and ISI, where $\overline{z}$ represents average of z for an arbitrary z (we also use $E(z)$ to indicate average of z, depending on the formula). We next summarize an analytical expression derived in [8] for the average Signal to Interference Ratio, as we will use it in the subsequent sections.

Theorem 1: (from [8]) The average Signal to Interference Ratio for $m > 0$, $SIR_{ave}^r = \frac{\overline{|\Gamma_0^r H_i X_i/N|^2}}{\overline{|I_i^r + S_i|^2}}$, will be as follows:

$$SIR_{ave}^r = \frac{(N-m)^2}{(2N-m)m - 2\frac{N-m}{\sigma_H^2} \sum_{k=0}^{m-1} \sum_{k'=k+1}^{C} \sigma_{h_{k'}}^2} \tag{11}$$

where $\sigma_H^2 = \overline{H_k H_k^*} = \sum_{i=0}^{C} \sigma_{h_i}^2$ with $\sigma_{h_i}^2$ representing the power of the i^{th} channel path, and H_k^* indicating conjugate of H_k.

Proof: See [8] for proof. ∎

B. Case of Timing Errors to the Left $(m < 0)$

In this case, due to the presence of the cyclic prefix, the number of data points that are missed can be less than $-m$. If the length of the channel delay spread spans C sampling periods, only $d = \max(C - (G+m), 0)$ data points are corrupted due to the interference from the previous symbol. Therefore,

$$y_i^l = \vartheta_{((i+m))_N} \times \gamma_i^l + \psi_i + w_i^l \quad 0 \le i \le N-1, \tag{12}$$

Where y_i^l is the i^{th} sample of the received signal for $m < 0$, $\psi_i = \begin{cases} y_{pf}(G+m+i) & 0 \le i \le d-1 \\ 0 & d \le i \le N-1 \end{cases}$ with $y_{pf}(i)$ representing the i^{th} sample of the output cyclic prefix of the current OFDM symbol (excluding the effect of AWGN), $\gamma_i^l = \begin{cases} 0 & 0 \le i \le d-1 \\ 1 & d \le i \le N-1 \end{cases}$ and w_i^l is a sample of AWGN. Then Y_i^l, the FFT of y_i^l, will be,

$$\begin{aligned} Y_i^l &= \frac{\Gamma_0^l}{N} H_i X_i e^{\frac{j2\pi mi}{N}} \\ &+ \underbrace{\overbrace{\sum_{k=1}^{N-1} \frac{\Gamma_k^l}{N} H_{((i-k))_N} X_{((i-k))_N} e^{\frac{j2\pi m(i-k)}{N}}}^{I_i^l} + \Psi_i + W_i^l}_{\text{ICI \& ISI}}, \end{aligned} \tag{13}$$

where Ψ_i is the FFT of ψ_i and Γ_i^l, the FFT of γ_i^l, is $\Gamma_i^l = \begin{cases} \frac{e^{-\frac{j2\pi id}{N}} - 1}{1 - e^{-\frac{j2\pi i}{N}}} & i \ne 0 \\ N-d & i = 0 \end{cases}$. Then, similar to the $m > 0$ case, average Signal to Interference Ratio, SIR_{ave}^l, will be as follows:

Theorem 2: (from [8]) The average Signal to Interference Ratio for $m < 0$, $SIR_{ave}^l = \frac{\overline{|\Gamma_0^l H_i X_i/N|^2}}{\overline{|I_i^l + \Psi_i|^2}}$, will be as follows:

$$SIR_{ave}^l = \frac{(N-d)^2}{(2N-d)d - 2\frac{N-d}{\sigma_H^2} \sum_{k=0}^{d-1} \sum_{k'=0}^{G+m+k} \sigma_{h_{k'}}^2} \tag{14}$$

Proof: See [8] for proof. ∎

IV. Effect of Timing Synchronization Errors on Pilot-Aided Channel Estimation

A. Case of $m > 0$

In this section we explore the effect of timing errors on the performance of a pilot-aided channel estimator discussed in Section II-B. Consider the case of $m > 0$. Let

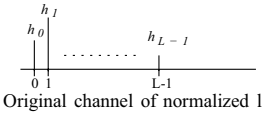

Fig. 1a Original channel of normalized length L − 1

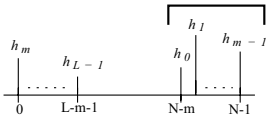

Fig. 1b Equivalent channel (m ≥ 1)

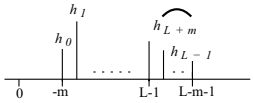

Fig. 1d Equivalent channel (m ≤ − 1)

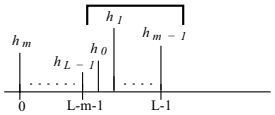

Fig. 1c Estimated eq. ch. (m ≥ 1)

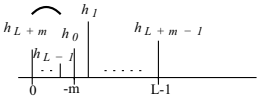

Fig. 1e Estimated eq. ch. (m ≤ − 1)

Fig. 1. Effect of rotations in different bases, the equivalent channel is rotated in base N, whereas the estimated equivalent channel is rotated in base L.

$H_{eq}(i) = \sum_k h_{eq}(k) e^{-\frac{j2\pi ik}{N}}$ represent the relationship between the transmitted data point at the i^{th} sub-carrier, X_i, and the received data point, Y_i^r in this case. Using Eq. 10, $H_{eq}^r(i) = \frac{\Gamma_0^r}{N} H_i e^{\frac{j2\pi mi}{N}}$ and

$$h_{eq}^r(k) = \underbrace{\frac{\Gamma_0^r}{N} h_{((k+m))_N}}_{\text{rotation in base } N}. \quad (15)$$

As can be seen, a timing synchronization error of $m > 0$ introduces a rotation of m sampling periods in the base of N in the equivalent channel. This rotation will result in the expansion of the channel beyond its maximum predicted length. To see this, Fig. 1b shows the equivalent channel for the original channel of length $L-1$ shown in Fig. 1a (L is defined in Section II). As can be seen, a rotation has occurred and resulted in the expansion of the equivalent channel beyond its maximum predicted length. Even an error of one sampling period to the right side results in an equivalent channel of length $N-1$. This will degrade the performance of the channel estimator, as it assumes an equivalent channel that spans $L-1$ sampling periods at maximum. To see the effect of timing errors on channel estimation analytically, consider the case that $L = \nu + 1$ equally-spaced frequency-domain pilot tones, $X_{pilot}(l_i)$ for $0 \le i \le L-1$, are inserted among the sub-carriers where $l_i = \frac{i \times N}{L}$. Then for $0 \le i \le L-1$,

$$\hat{H}_{eq}^r(l_i) = \frac{Y_{l_i}^r}{X_{pilot}(l_i)} = H_{eq}^r(l_i) + \frac{I_{l_i}^r + S_{l_i} + W_{l_i}^r}{X_{pilot}(l_i)}. \quad (16)$$

After an IFFT of length L, the estimate of the channel in the time domain will be

$$\hat{h}_{eq}^r(k) = \underbrace{\frac{\Gamma_0^r}{N} h_{((k+m))_L}}_{\text{rotation in base } L} + \underbrace{u_k^r}_{\text{Interference}} + \underbrace{v_k^r}_{\text{AWGN}}. \quad (17)$$

Define U_i^r and V_i^r as follows:

$$U_i^r = \sum_{z=0}^{L-1} \alpha_{i,z} \frac{I_{l_z}^r + S_{l_z}}{X_{pilot}(l_z)} \quad \& \quad V_i^r = \sum_{z=0}^{L-1} \alpha_{i,z} \frac{W_{l_z}^r}{X_{pilot}(l_z)}. \quad (18)$$

Then u^r and v^r will be the IFFTs of U^r and V^r respectively and $\alpha_{i,z} = \frac{1}{L} \sum_{g=0}^{L-1} e^{j2\pi g(\frac{z}{L} - \frac{i}{N})}$.

By comparing Eq. 17 with Eq. 15, it can be seen that there are three factors contributing to the channel estimation error: rotations in different bases, interference and noise. The first factor occurs because the equivalent channel has a rotation in the base of N while the estimated equivalent channel has a rotation in the base of L. Since L is chosen based on the maximum predicted length of the original channel, $\nu \le G$, it is typically considerably smaller than N. Therefore, the mismatch between the equivalent channel and the estimated equivalent channel can be considerable, solely due to the first factor. Fig. 1c shows the estimated equivalent channel for the equivalent channel of Fig. 1b (effect of interference and noise is not shown on the figure). By comparing Fig. 1b and 1c, a mismatch can be observed in the location of the first m paths of the original channel. Since these samples are typically strong, this can result in a considerable performance degradation of the channel estimator[1]. To analytically assess the contribution of each of the aforementioned factors, we next derive an analytical expression for the average channel estimation error variance. Channel estimation error will be as follows for $0 \le i \le N-1$,

$$\Delta H_{eq}^r(i) = \underbrace{\sum_{k=0}^{m-1} \beta_{i,k}^r h_k}_{\text{rotations in different bases}} + \underbrace{U_i^r}_{\text{interference}} + \underbrace{V_i^r}_{\text{AWGN}}, \quad (19)$$

where ΔH_{eq}^r represents the frequency-domain channel estimation error for $m > 0$ and $\beta_{i,k}^r = \frac{N-m}{N} \times e^{\frac{-j2\pi i(k-m)}{N}} \times (1 - e^{-\frac{j2\pi iL}{N}})$.

Theorem 3: Consider an OFDM system with a timing synchronization error of m sampling periods to the right. Let $Ch_{error,norm}^r(i)$ represent the normalized average channel estimation error variance of the pilot-aided channel estimator discussed in Section II: $Ch_{error,norm}^r(i) = \frac{\overline{|\Delta H_{eq}^r(i)|^2}}{\overline{|H_{eq}^r(i)|^2}}$. Then we will have,

$$Ch_{error,norm}^r(i) = \underbrace{4 \frac{\sum_{k=0}^{m-1} \sigma_{h_k}^2 - \frac{\sum_{k=1}^{m-1} k\sigma_{h_k}^2}{N-m} \varpi(m-2)}{\sum_{k=0}^{C} \sigma_{h_k}^2} sin^2(\frac{\pi iL}{N}) +}_{\text{factor\#1: rotations in different bases}}$$
$$\underbrace{\frac{1}{SIR_{ave}^r(m)}}_{\text{interference}} + \underbrace{\frac{1}{SNR_{ave}^r(m)}}_{\text{noise}}, \quad (20)$$

where $SNR_{ave}^r(m) = \frac{(N-m)^2 \sigma_X^2 \sigma_H^2}{N^2 \sigma_W^2}$ and $\varpi(z) = 1$ for $z \ge 0$ and zero otherwise. σ_H^2 and C are as defined in Section III, $\overline{X_i X_j^*} = \sigma_X^2 \delta_{ij}$ and σ_W^2 is the variance of W_i.

Proof: Using the definition of $I_{l_z}^r$ from Eq. 10, we will have $\overline{\left[\frac{I_{l_z}^r h_k^*}{X_{pilot}(l_z)}\right]} = \sum_{k'=1}^{N-1} \frac{\Gamma_{k'}^r}{N} \overline{H_{((l_z-k'))_N} h_k^* \left[\frac{X_{((l_z-k'))_N}}{X_{pilot}(l_z)}\right]} e^{\frac{j2\pi m(l_z-k')}{N}}$ for $0 \le z \le L-1$ and $0 \le k \le m-1$. Noting that $X_{pilot}(l_z) = X_{l_z}$ will result in $\left[\frac{X_{((l_z-k'))_N}}{X_{pilot}(l_z)}\right] = 0$ for

[1]It should be noted that the estimated equivalent channel is not a rotated version of the equivalent channel. Therefore their Fourier transforms, i.e. H_{eq}^r and $\hat{H}_{eq}^r$, differ both in amplitude and phase.

$1 \leq k' \leq N-1$ and iid Xs. Therefore,

$$\overline{\left[\frac{I^r_{l_z} h^*_k}{X_{pilot}(l_z)}\right]} = 0 \quad \text{for} \quad 0 \leq z \leq L-1 \quad 0 \leq k \leq m-1. \tag{21}$$

Then we will have the following using Eq. 18,

$$\overline{U^r_i h^*_k} = \sum_{z=0}^{L-1} \alpha_{i,z} \overline{\left[\frac{S_{l_z} h^*_k}{X_{pilot}(l_z)}\right]} = \sum_{k'=0}^{m-1} \sum_{k''=k'+1}^{C} \overline{h_{k''} h^*_k} \sum_{z=0}^{L-1} \alpha_{i,z} \overline{\left[\frac{x_{N-k''+k'}}{X_{pilot}(l_z)}\right]} e^{-\frac{j2\pi(k'-m)z}{L}} = \frac{1}{N} \sum_{k'=0}^{m-1} \sum_{k''=k'+1}^{C} \overline{h_{k''} h^*_k} \sum_{z=0}^{L-1} \alpha_{i,z} e^{-\frac{j2\pi[(k'-m)z-(k'-k'')z]}{L}} = \frac{1}{N} \left[\sum_{k''=1}^{m-1} k'' \overline{h_{k''} h^*_k} + m \sum_{k''=m}^{C} \overline{h_{k''} h^*_k}\right] \times \sum_{z=0}^{L-1} \alpha_{i,z} e^{-\frac{j2\pi(k''-m)z}{L}}. \tag{22}$$

Since we are interested in $\overline{U^r_i h^*_k}$ for $0 \leq k \leq m-1$, the second term in the bracket is zero. Therefore,

$$\overline{U^r_i h^*_k} = \begin{cases} \frac{k}{N} \sigma^2_{h_k} \sum_{z=0}^{L-1} \alpha_{i,z} e^{-\frac{j2\pi(k-m)z}{L}} & k \geq 1 \\ 0 & k = 0 \end{cases} \tag{23}$$

and

$$\sum_{k=0}^{m-1} \beta^{*r}_{i,k} \overline{U^r_i h^*_k} = \frac{1}{N} \sum_{k=1}^{m-1} k \sigma^2_{h_k} \beta^{*r}_{i,k} \sum_{z=0}^{L-1} \alpha_{i,z} e^{-\frac{j2\pi(k-m)z}{L}} = \frac{1}{NL} \sum_{k=1}^{m-1} k \sigma^2_{h_k} \beta^{*r}_{i,k} \sum_{z'=0}^{L-1} \sum_{z=0}^{L-1} e^{\frac{j2\pi(z'-k+m)z}{L}} e^{-\frac{j2\pi z' i}{N}}. \tag{24}$$

Since $1 \leq z'-k+m \leq L-2+m$, Eq. 24 will be non-zero only if $z'-k+m = L$ and $m \geq 2$. Since for any k in the given range of Eq. 24, $0 \leq L+k-m \leq L-1$ for $2 \leq m \leq L+1$, there will always exist a z' that will make $z'-k+m = L$. Therefore, $\sum_{k=0}^{m-1} \beta^{*r}_{i,k} \overline{U^r_i h^*_k} = \frac{1}{N} \sum_{k=1}^{m-1} k \sigma^2_{h_k} \beta^{*r}_{i,k} e^{-\frac{j2\pi(L+k-m)i}{N}}$ for $m \geq 2$. Then,

$$\sum_{k=0}^{m-1} \beta^{*r}_{i,k} \overline{U^r_i h^*_k} = \begin{cases} \frac{(N-m)\times(e^{-\frac{j2\pi Li}{N}}-1)}{N^2} \sum_{k=1}^{m-1} k \sigma^2_{h_k} & m \geq 2 \\ 0 & m = 1 \end{cases} \tag{25}$$

Noting that the Gaussian noise term is independent of the first two terms on the right hand side of Eq. 19 results in the following expression:

$$\overline{|\Delta H^r_{eq}(i)|^2} = \sum_{k=0}^{m-1} |\beta^r_{i,k}|^2 \sigma^2_{h_k} + \sigma^2_{U^r_i} + \sigma^2_{V^r_i} + 2\Re\{\sum_{k=0}^{m-1} \beta^{*r}_{i,k} \overline{U^r_i h^*_k}\}, \tag{26}$$

where $\Re\{.\}$ represents the real part of the argument. We will have $|\beta^r_{i,k}|^2 = 4\frac{(N-m)^2}{N^2} sin^2(\frac{\pi i L}{N})$, using the expression of β^r from Eq. 19, and $\sigma^2_{V^r_i} = \frac{\sigma^2_W}{\sigma^2_X}$. An expression for $\sigma^2_{U^r_i}$ is derived next.

$$\sigma^2_{U^r_i} = \sum_{z=0}^{L-1} \sum_{z'=0, z' \neq z}^{L-1} \alpha_{i,z} \alpha^*_{i,z'} E\left[\frac{(I^r_{l_z}+S_{l_z})\times(I^{r*}_{l_{z'}}+S^*_{l_{z'}})}{X_{pilot}(l_z) X^*_{pilot}(l_{z'})}\right] + \sum_{z=0}^{L-1} |\alpha_{i,z}|^2 \frac{\overline{|I^r_{l_z}+S_{l_z}|^2}}{\sigma^2_X}. \tag{27}$$

Next we calculate $E\left[\frac{I^r_{l_z} \times I^{r*}_{l_{z'}}}{X_{pilot}(l_z) X^*_{pilot}(l_{z'})}\right]$. $E\left[\frac{I^r_{l_z} \times I^{r*}_{l_{z'}}}{X_{pilot}(l_z) X^*_{pilot}(l_{z'})}\right]$ involves evaluating $E\left[\frac{X_{((l_z-k))_N} X^*_{((l_{z'}-k'))_N}}{X_{pilot}(l_z) X^*_{pilot}(l_{z'})}\right]$ for $1 \leq k, k' \leq N-1$ and $z \neq z'$. For $1 \leq k, k' \leq N-1$ and $z \neq z'$, we will have $((l_z-k))_N \neq l_z$, $((l_{z'}-k))_N \neq l_{z'}$ and $l_z \neq l_{z'}$. Therefore, If $((l_z-k))_N = ((l_{z'}-k'))_N$, $E\left[\frac{X_{((l_z-k))_N} X^*_{((l_{z'}-k'))_N}}{X_{pilot}(l_z) X^*_{pilot}(l_{z'})}\right] = E(\frac{|X_{((l_z-k))_N}|^2}{X^*_{l_{z'}}}) \times \overline{\left[\frac{1}{X_{l_z}}\right]}$ for iid Xs (note that $X_{pilot}(g) = X_g$). For zero-mean constellations (such as PSK or QAM), it can be easily verified that $\overline{\left[\frac{1}{X_{l_z}}\right]} = 0$ (for instance in QAM, if X is a point in the constellation, $Xe^{j\pi}$ is also a point in constellation). Therefore, $\overline{\left[\frac{1}{X_{l_z}}\right]}$ is zero resulting in $E\left[\frac{X_{((l_z-k))_N} X^*_{((l_{z'}-k'))_N}}{X_{pilot}(l_z) X^*_{pilot}(l_{z'})}\right] = 0$. Lets consider the cases where $((l_z-k))_N \neq ((l_{z'}-k'))_N$. If $((l_z-k))_N = l_{z'}$ and $((l_{z'}-k'))_N \neq l_z$ or $((l_{z'}-k'))_N = l_z$ and $((l_z-k))_N \neq l_{z'}$, then it can be easily verified that $E\left[\frac{X_{((l_z-k))_N} X^*_{((l_{z'}-k'))_N}}{X_{pilot}(l_z) X^*_{pilot}(l_{z'})}\right] = 0$. If $((l_z-k))_N = l_{z'}$ and $((l_{z'}-k'))_N = l_z$, then $E\left[\frac{X_{((l_z-k))_N} X^*_{((l_{z'}-k'))_N}}{X_{pilot}(l_z) X^*_{pilot}(l_{z'})}\right] = E\left[\frac{X_{l_{z'}}}{X^*_{l_{z'}}}\right] \times E\left[\frac{X^*_{l_z}}{X_{l_z}}\right]$. It can be easily verified that $E\left[\frac{X}{X^*}\right]$ is zero for MPSK modulations with $M > 2$ and QAM modulations. To see this divide the constellation points into sub-groups with equal amplitudes. It can be easily shown that $E\left[\frac{X}{X^*}\right]$ will be zero for each sub-group. Note that for PAM modulations $E\left[\frac{X}{X^*}\right]$ equals one. However, since PSK and QAM modulations are commonly used, we will proceed with that assumption to facilitate mathematical derivations[2]. Therefore, $E\left[\frac{X_{((l_z-k))_N} X^*_{((l_{z'}-k'))_N}}{X_{pilot}(l_z) X^*_{pilot}(l_{z'})}\right] = 0$ and $E\left[\frac{I^r_{l_z} \times I^{r*}_{l_{z'}}}{X_{pilot}(l_z) X^*_{pilot}(l_{z'})}\right] = 0$.

Next the following expression can be written for $g \neq g'$,

$$\overline{\left[\frac{I^r_g S^*_{g'}}{X_g X^*_{g'}}\right]} = \sum_{k=0}^{m-1} \sum_{k'=k+1}^{C} \sum_{k''=1}^{N-1} \frac{\Gamma^r_{k''}}{N} \overline{H_{((g-k''))_N} h^*_{k'}} \overline{\left[\frac{X_{((g-k''))_N} x^*_{N-k'+k}}{X_g X^*_{g'}}\right]} e^{\frac{j2\pi[g'(k-m)+m(g-k'')]}{N}}. \tag{28}$$

Since $k'' \geq 1$, we will have the following for $g \neq g'$,

$$\overline{\left[\frac{X_{((g-k''))_N} x^*_{N-k'+k}}{X_g X^*_{g'}}\right]} = \frac{1}{N} \sum_{k'''=0}^{N-1} \overline{\left[\frac{X^*_{k'''} X_{((g-k''))_N}}{X_g X^*_{g'}}\right]} e^{\frac{-j2\pi k'''(k-k')}{N}} = 0. \tag{29}$$

[2] $E\left[\frac{I^r_{l_z} \times I^{r*}_{l_{z'}}}{X_{pilot}(l_z) X^*_{pilot}(l_{z'})}\right]$ can be easily characterized for PAM modulations.

Therefore,

$$E\left[\frac{I_g^r S_{g'}^*}{X_g X_{g'}^*}\right] = 0 \quad g \neq g'. \tag{30}$$

Then Eq. 27 can be written as follows:

$$\begin{aligned}\sigma_{U_i^r}^2 &= \sum_{z=0}^{L-1}\sum_{z'=0,z'\neq z}^{L-1} \alpha_{i,z}\alpha_{i,z'}^* E\left[\frac{S_{l_z}S_{l_{z'}}^*}{X_{pilot}(l_z)X_{pilot}^*(l_{z'})}\right] \\ &+ \sum_{z=0}^{L-1}|\alpha_{i,z}|^2\frac{\overline{|I_{l_z}^r+S_{l_z}|^2}}{\sigma_X^2}.\end{aligned} \tag{31}$$

For an arbitrary k'' and g'' where $k'' \neq g''$, the following expression can be written,

$$E\left[\frac{S_{k''}S_{g''}^*}{X_{k''}X_{g''}^*}\right] = E\left[\frac{\sum_{k=0}^{m-1} s_{N-m+k}e^{\frac{-j2\pi k''(k-m)}{N}}\sum_{g=0}^{m-1} s_{N-m+g}^* e^{\frac{j2\pi g''(g-m)}{N}}}{X_{k''}X_{g''}^*}\right]. \tag{32}$$

Using the expression of s from Section III and noting that the ICI and ISI terms of Eq. 9 are independent,

$$\begin{aligned}&E\left[\frac{S_{k''}S_{g''}^*}{X_{k''}X_{g''}^*}\right] = \\ &\frac{\sum_{k=0}^{m-1}\sum_{g=0}^{m-1}\sum_{k'=k+1}^{C}\sum_{g'=g+1}^{C}}{\overline{h_{k'}h_{g'}^*}\left[\frac{x_{N-k'+k}x_{N-g'+g}^*}{X_{k''}X_{g''}^*}\right]} \times e^{\frac{-j2\pi[(k-m)k''-(g-m)g'']}{N}} = \\ &\frac{1}{N^2}\sum_{k=0}^{m-1}\sum_{g=0}^{m-1}\sum_{k'=max(k,g)+1}^{C}\sigma_{h_{k'}}^2 e^{-\frac{j2\pi(k'-m)(k''-g'')}{N}} \\ &\text{for} \quad k''\neq g''.\end{aligned} \tag{33}$$

Therefore, the first term on the right hand side of Eq. 31 can be written as follows:

$$\begin{aligned}&\sum_{z=0}^{L-1}\sum_{z'=0,z'\neq z}^{L-1}\alpha_{i,z}\alpha_{i,z'}^* E\left[\frac{S_{l_z}S_{l_{z'}}^*}{X_{pilot}(l_z)X_{pilot}^*(l_{z'})}\right] = \\ &\frac{1}{N^2L^2}\sum_{k=0}^{m-1}\sum_{g=0}^{m-1}\sum_{k'=max(k,g)+1}^{C}\sigma_{h_{k'}}^2 \times \\ &\sum_{g'=0}^{L-1}\sum_{g''=0}^{L-1} e^{-\frac{j2\pi i(g'-g'')}{N}} \times \\ &\left[\sum_{z=0}^{L-1} e^{\frac{j2\pi z(g'-k'+m)}{L}}\sum_{z'=0}^{L-1} e^{-\frac{j2\pi z'(g''-k'+m)}{L}} - \right. \\ &\left.\sum_{z=0}^{L-1} e^{\frac{j2\pi z(g'-g'')}{L}}\right].\end{aligned} \tag{34}$$

Since $-L < -C+m \leq g'-k'+m \leq L-2+m$, then $-L < -C+m \leq g'-k'+m \leq 2L-1$ for $m \leq L+1$. Therefore, the first two sums inside the bracket will have non-zero values only for $g'-k'+m = L$ and 0. In order to have $g'-k'+m = 0$ and $g'-k'+m = L$, $0 \leq k'-m \leq L-1$ and $-L \leq k'-m \leq -1$ should hold respectively. Therefore, for $-L \leq k'-m \leq L-1$, there will always be a g' in the range of $0 \leq g' \leq L-1$. We have $1 \leq k' \leq C$ in Eq. 34. For any k' in this range, $-L \leq k'-m \leq L-1$ (assuming that $m \leq L+1$). Then for any k' of Eq. 34, there exists one and only one g' that would result in $g'-k'+m$ to be a multiple of L (here only 0 or L). Therefore, $\sum_{z=0}^{L-1}\sum_{z'=0,z'\neq z}^{L-1}\alpha_{i,z}\alpha_{i,z'}^* E\left[\frac{S_{l_z}S_{l_{z'}}^*}{X_{pilot}(l_z)X_{pilot}^*(l_{z'})}\right] = 0$. Then, $\sigma_{U_i^r}^2 = \sum_{z=0}^{L-1}|\alpha_{i,z}|^2\frac{\overline{|I_{l_z}^r+S_{l_z}|^2}}{\sigma_X^2}$. It can be easily proved that $\forall i, \sum_{z=0}^{L-1}|\alpha_{i,z}|^2 = 1$. Then using the definition of SIR_{ave}^r of Theorem 1, we will have,

$$\sigma_{U_i^r}^2 = \left(\frac{N-m}{N}\right)^2 (SIR_{ave}^r)^{-1}\sigma_H^2. \tag{35}$$

Using Eq. 25 and 26, $\overline{|\Delta H_{eq}^r(i)|^2}$ will then be as follows:

$$\begin{aligned}&\overline{|\Delta H_{eq}^r(i)|^2} = \\ &\sum_{k=0}^{m-1}|\beta_{i,k}^r|^2\sigma_{h_k}^2 + \sigma_{U_i^r}^2 + \sigma_{V_i^r}^2 + 2\Re\{\sum_{k=0}^{m-1}\beta_{i,k}^{*r}\overline{U_i^r h_k^*}\} \\ &= 4\frac{(N-m)^2}{N^2}sin^2\left(\frac{\pi iL}{N}\right)\sum_{k=0}^{m-1}\sigma_{h_k}^2 \\ &+\left(\frac{N-m}{N}\right)^2(SIR_{ave}^r)^{-1}\sigma_H^2 + \frac{\sigma_W^2}{\sigma_X^2} \\ &-\frac{4(N-m)sin^2\left(\frac{\pi iL}{N}\right)\sum_{k=1}^{m-1}k\sigma_{h_k}^2}{N^2}\varpi(m-2),\end{aligned} \tag{36}$$

where $\varpi(z) = 1$ for $z \geq 0$ and zero otherwise. Then the normalized average channel estimation error variance at the i^{th} sub-carrier, $Ch_{error,norm}^r(i)$, can be written as follows:

$$\begin{aligned}Ch_{error,norm}^r(i) &= \frac{\overline{|\Delta H_{eq}^r(i)|^2}}{|H_{eq}^r(i)|^2} \\ &= \underbrace{4\frac{\sum_{k=0}^{m-1}\sigma_{h_k}^2 - \frac{\sum_{k=1}^{m-1}k\sigma_{h_k}^2}{N-m}\varpi(m-2)}{\sum_{k=0}^{C}\sigma_{h_k}^2}sin^2\left(\frac{\pi iL}{N}\right)}_{\text{factor\#1: rotations in different bases}} \\ &+ \underbrace{\frac{1}{SIR_{ave}^r(m)}}_{\text{interference}} + \underbrace{\frac{1}{SNR_{ave}^r(m)}}_{\text{noise}},\end{aligned} \tag{37}$$

where $SNR_{ave}^r(m) = \frac{(N-m)^2\sigma_X^2\sigma_H^2}{N^2\sigma_W^2}$. ■

Since, with high probability, m is considerably smaller than N, Eq. 37 can be tightly approximated. For m considerably smaller than N, $\frac{k}{N-m} \ll 1$ for $1 \leq k \leq m-1$. Therefore,

$$\begin{aligned}Ch_{error,norm}^r(i) &\approx \underbrace{4\Upsilon_{\%}^r(m)sin^2\left(\frac{\pi iL}{N}\right)}_{\text{factor\#1: rotations in different bases}} \\ &+ \underbrace{\frac{1}{SIR_{ave}^r(m)}}_{\text{interference}} + \underbrace{\frac{1}{SNR_{ave}^r(m)}}_{\text{noise}},\end{aligned} \tag{38}$$

where $\Upsilon_{\%}^r(m) = \frac{\sum_{k=0}^{m-1}\sigma_{h_k}^2}{\sum_{k=0}^{C}\sigma_{h_k}^2}$ represents the ratio of the power of the misplaced channel paths to the total power of the channel (see Fig. 1b, c). Let *factor#1* represent the effect of rotation (first term on the right-hand side of Eq. 38). As expected, it does not affect those sub-channels carrying pilot tones. However, it results in a considerable increase of error for other sub-carriers particularly for those at $i = z_{odd} \times \text{ceil}(\frac{N}{2L})$, where z_{odd} represents odd integers and ceil(.) represents the ceiling function. In a reasonable SNR_{ave}^r environment, the overall impact of *factor#1* is considerably higher than other terms. Let $Ch_{error,ratio}$ represent the ratio of the first term to the sum of the last two terms on the right hand side of Eq. 38. Examining $Ch_{error,ratio}$ for different values of m and $\Upsilon_{\%}^r$ in a reasonable SNR environment shows that *factor#1* is the dominant factor with high probability.

B. Case of $m < 0$

Similar expressions can be derived for the case of $m < 0$. Using Eq. 13, $H_{eq}^l(i) = \frac{\Gamma_0^l}{N}H_i e^{\frac{j2\pi mi}{N}}$ and $h_{eq}^l(k) = \frac{\Gamma_0^l}{N}h_{((k+m))_N}$. To see the effect of rotations in different bases

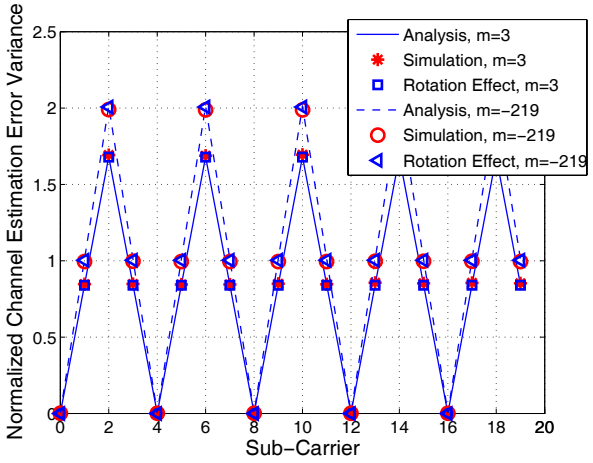

Fig. 2. Normalized channel estimation error variance vs. sub-carrier for $m = 3$ ($\Upsilon^r_{\%} = 42\%$) and $m = -219$ ($\Upsilon^l_{\%} = 50\%$).

in this case, Fig. 1d and 1e show the equivalent and estimated equivalent channel for the original channel of Fig. 1a respectively. Unlike the case of $m > 0$, where even one error to the right resulted in an equivalent channel of length $N-1$ (see Fig. 1b), the equivalent channel length for $m < 0$ varies depending on the length of the original channel. For instance, for a channel of length $C \leq \nu$, the equivalent channel length will be $C - m$ for $m \leq -1$. Therefore for $C - \nu \leq m \leq -1$, the equivalent length would still be less than or equal to ν, which poses no problem for the channel estimator. Note that ν is the maximum normalized predicted channel delay spread as defined in Section II-B. Furthermore, the mismatch is in the location of the last m paths of the original channel and these samples are not typically that strong. Therefore, errors to the left side may not degrade the performance (both in terms of effect of rotation and interference), depending on the length of the channel delay spread, length of the guard interval and number of pilot tones. Following the same procedure, an analytical expression can be found for the case of $m < 0$. Let $Ch^l_{error,norm}(i)$ represent the normalized average channel estimation error variance for $m < 0$. Then it can be tightly approximated as follows,

$$Ch^l_{error,norm}(i) \approx \underbrace{4sin^2(\frac{\pi i L}{N})\Upsilon^l_{\%}(m)}_{\text{factor\#1: rotations in different bases}} + \underbrace{\frac{1}{SIR^l_{ave}(m)}}_{\text{interference}} + \underbrace{\frac{1}{SNR^l_{ave}(m)}}_{\text{noise}}, \quad (39)$$

where $\Upsilon^l_{\%}(m) = \frac{\sum_{k=L+m}^{L-1} \sigma^2_{h_k}}{\sum_{k=0}^{C} \sigma^2_{h_k}}$ represents the ratio of the power of the misplaced channel paths to the total power of the channel for the case of $m < 0$, $SNR^l_{ave}(m) = \frac{(N-d)^2 \sigma^2_X \sigma^2_H}{N^2 \sigma^2_W}$ and d is as defined in Section III-B.

C. Simulation Results

As can be seen from the expressions for the average channel estimation error variance, timing errors can degrade the performance of a pilot-aided channel estimator considerably. Furthermore, *factor#1*, the effect of rotations in different bases, is the major contributor to channel estimation error. Fig. 2 shows normalized average channel estimation error variance, from both analysis and simulations, as a function of sub-carrier and for a channel with the following power-delay profile: $[0.1214 \quad 0.1969 \quad 0.0987 \quad 0.0784 \quad 0.1242 \quad 0.1969 \quad 0.0987 \quad 0.0623 \quad 0.0197]$. System specifications are as follows for this result: $N = 892$ and $G = L = 223$. The channel is estimated using the pilot tones inserted at locations 0, 4, 8, ... As can be seen, for both cases of $m > 0$ and $m < 0$, *factor#1* (rotations in different bases) contributes almost all the channel estimation error. Furthermore, it can be seen that channel estimation error can be considerably high in the presence of timing errors. Finally, simulation results verify mathematical derivations of this section.

V. Timing Synchronization Error Correction

It was shown that the pilot-aided channel estimator is considerably sensitive to timing synchronization errors due to the effect of rotations in different bases. This sensitivity can be exploited to design a robust synchronization algorithm that requires no training information. After a coarse timing synchronizer has detected a start point for the OFDM symbol (different choices for this synchronizer will be discussed later in this section), $\hat{H}_{eq}(k)$ can be obtained using the pilot tones. This channel estimate may be far from $H_{eq}(k)$ in the presence of timing errors . Let $\hat{X}_k = \frac{Y_k}{\hat{H}_{eq}(k)}$ and $\tilde{X}_k = Dec(\hat{X}_k)$ represent the estimated input before and after the decision device respectively. Define a decision-directed measure function as $MF = \sum_{k=0}^{N-1} |\hat{X}_k - \tilde{X}_k|^2$. In the presence of *factor#1*, MF can be considerably high. Therefore, synchronization errors can be detected and corrected by minimizing MF. As long as *factor#1* is the major cause of performance loss, which is the case with high probability, we can detect timing errors. Due to the nature of *factor#1*, it is possible to perform all the updates necessary for detecting and correcting timing errors in the frequency-domain, without a need to go back and forth from the frequency to the time domain. Consider correcting errors to the right. As can be seen from Fig. 1c, the position of the last m paths of the estimated equivalent channel is different from that of the equivalent channel, where m is unknown. We update the estimated equivalent channel through an iterative process, correcting for one mismatched channel path at a time. This means that in the first iteration, the last channel path in $\hat{h}^r_{eq}(k)$ should be transferred from position $L-1$ to position $N-1$. Following the same procedure, the update necessary at the k^{th} sub-channel to correct errors to the right will be as follow in the i^{th} iteration ($i \geq 1$) (a channel path is moved from position $L-i$ to $N-i$):

$$\hat{H}^{(i+1),r}_{eq}(k) = \hat{H}^{(i),r}_{eq}(k) + \varsigma \times \hat{h}^r_{eq}(L-i) \times e^{\frac{j2\pi ik}{N}}. \quad (40)$$

Similarly we will have the following for detecting errors to the left,

$$\hat{H}^{(i+1),l}_{eq}(k) = \hat{H}^{(i),l}_{eq}(k) - \varsigma \times \hat{h}^l_{eq}(i-1) \times e^{-\frac{j2\pi(i-1)k}{N}}, \quad (41)$$

Where $\varsigma = 1 - e^{-\frac{j2\pi Lk}{N}}$ and $\hat{H}^{(1),r}_{eq}(k) = \hat{H}^r_{eq}(k)$ and $\hat{H}^{(1),l}_{eq}(k) = \hat{H}^l_{eq}(k)$. In each iteration, the measure function, $MF^{(i)}$, will be evaluated. Finally the iteration that results

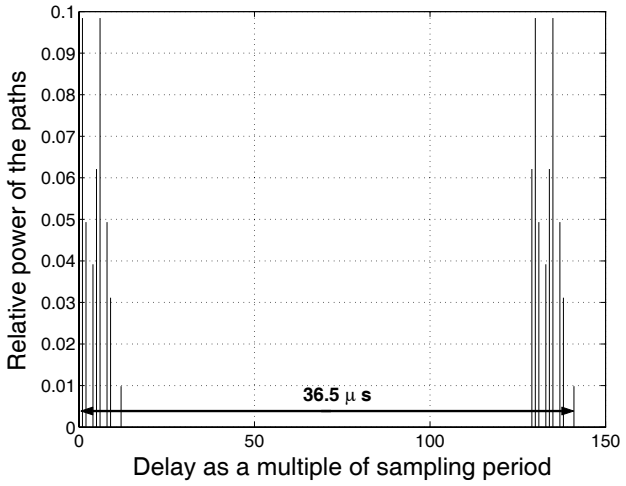

Fig. 3. Power-delay profile of channel#1.

in the minimum MF, or MF below a predefined threshold, is selected[3]. Call this iteration $i_{corr,z}$, where $z = 1$ denotes that a timing error to the right has been detected. Similarly $z = -1$ indicates detection of an error to the left. Then it is possible to go back to the time domain and correct the start of the symbol. For $z = 1$, the initial start point of the symbol should be moved to the left by $i_{corr,z}$. The opposite will be the case for $z = -1$. In practice, a coarse synchronizer could be used for the initial timing synchronization. A traditional choice would be a sliding correlator that correlates the data points at the beginning and end of the symbol, looking for a peak [19]. This will be then followed by the proposed fine synchronization algorithm. Since the proposed algorithm works robustly, there is no requirement on the quality of the initial coarse synchronization (as long as $|m| < L$) and is used solely to have a start point for the proposed algorithm.

Note that the sensitivity of the pilot-aided channel estimator to *factor#1* makes it possible to design a timing synchronizer with a considerably better performance than the traditional one, without relying on synchronization training information. Furthermore, it allows for timing error detection solely in the frequency domain which reduces the complexity considerably, compared to going back and forth from frequency to time domain. If a sub-optimum channel estimator were to be used instead, the same improvement would not be achieved for two reasons. First, the high sensitivity of the pilot-aided channel estimator to timing synchronization errors allows for robust detection and correction of synchronization errors in the presence of noise and Doppler. However, such sensitivity does not exist for other sub-optimum estimators, resulting in a rather high probability of false detection in the fine synchronization stage. Second, due to the lack of *factor#1* for other estimators, timing synchronization errors do not affect the estimated channel significantly. Therefore detecting the timing error solely in the frequency domain, as was done in the proposed algorithm, would not result in timing error detection. Then to perform a decision-directed correction, there would be a need to go back and forth between time and frequency domains, which would increase the complexity considerably without resulting in an acceptable performance.

[3]Unless it is known apriori that m is positive or negative, both directions should be tried.

VI. Simulation Results

An OFDM system is simulated in a high delay spread fading environment of a Single Frequency Network[4] (SFN). SFN refers to the networks such as DAB and DVB that broadcast on the same frequency in adjacent cells and therefore can experience considerably high delay spreads. The following parameters are chosen for simulations[5]. Input modulation is 8PSK. Useful bit rate is 7.3Mbps. N=892, $L = G$=223 and $T_s = .26\mu s$. The power-delay profile of the simulated channels have two main clusters each with 9 non-zero paths, to represent an SFN channel. Two power-delay profiles are considered. Power-delay profile of Channel#1, shown in Fig. 3, has delay spread of $36.5\mu s$, spanning 64% of the guard interval. Channel#2 has a similar profile, but the delay between its two clusters has increased such that the total length spans 100% of the guard interval (worst case channel) in order to make the impact of errors to the left side more pronounced. In both channels two clusters have equal power as can be seen from Fig. 3. Each channel path is generated as a random variable with Rayleigh distributed amplitude and uniformly distributed phase [7], [15]. Three methods are simulated. The first two methods are based on the traditional correlation-based timing synchronization, using the redundancy of the cyclic prefix. Method I is method of Van de Beek et al., [19], which picks the maximum correlation point. Method II is basically method I with a simple variation to improve the performance. It picks the point from which the sum of the next L correlation points is maximized, hence reducing the chance of an error to the right side (which is more costly) at the price of increasing the probability of errors to the left side. Method III utilizes method I for initial coarse synchronization followed by our proposed synchronization error correction method of the previous section. The initial uncertainty range for the start of the OFDM symbol is taken to be from the middle of the previous symbol to the middle of the next symbol. To evaluate the performance of these methods, $P_{error}(m)$, the average probability of making a timing error of m sampling periods, is measured. To evaluate the cost of making an erroneous offset, we use $P_b(m)$, the average BER (Bit Error Rate) in case of an offset of m sampling periods (this is the pre-decoding BER).

The first and third curves of Fig. 4 show $P_{error}(m)$ of the three methods, for channel#1 in the absence of noise. The second and fourth curves of Fig. 4 show $P_b(m)$ for the three methods[6]. The delay spread of channel#1 spans 64% of the guard interval. This allows for timing offsets of up to 36% of the guard interval (which becomes 82 sampling points) to the left to occur without any loss of performance.

[4]Similar (or more) improvement is also obtained with non-SFN channels.

[5]System parameters are based on the Sirius Radio second generation system specification.

[6]Note that $P_b(m)$ of method III is different from that of method I and II. To obtain $P_b(m)$ at a specific timing synchronization offset, bit error rate should be averaged over different input, noise and channel realizations at that synchronization offset. For a given offset of m, channel realizations that would lead to that offset are different for method III than those for methods I and II. This is due to the fact that method III uses channel estimation to correct timing errors.

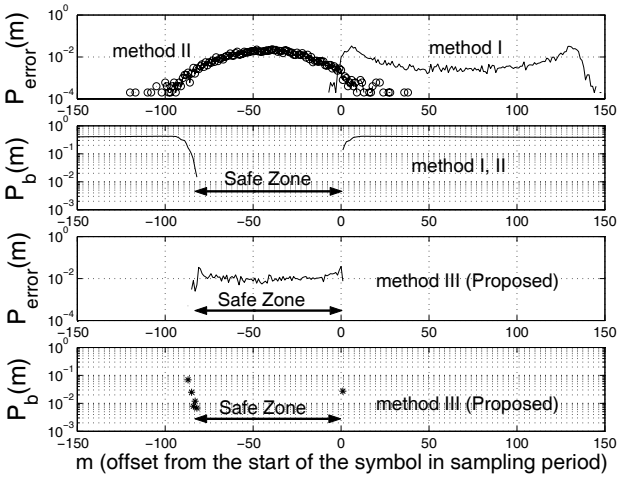

Fig. 4. Performance of the proposed timing synchronizer for channel#1 in the absence of noise.

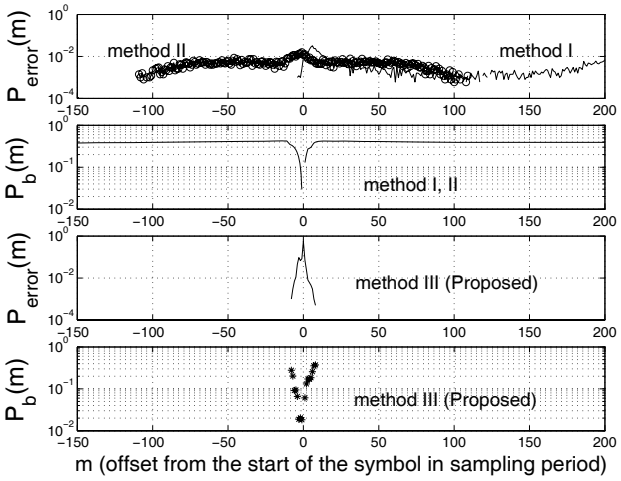

Fig. 5. Performance of the proposed timing synchronizer for channel#2 in the absence of noise.

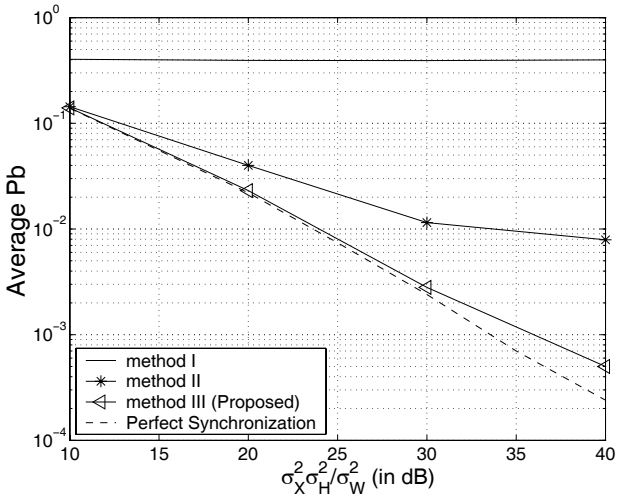

Fig. 6. Average P_b for channel#1 in the presence of noise.

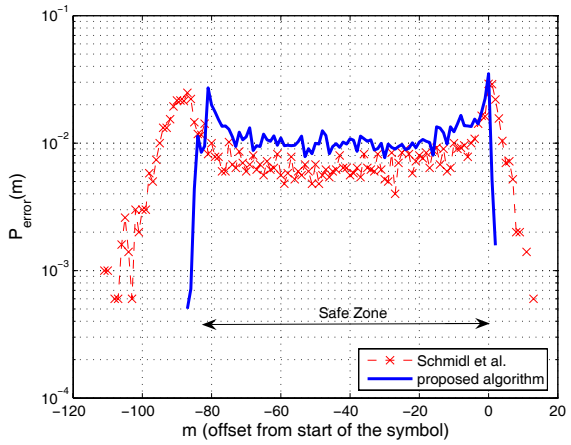

Fig. 7. Comparison with the algorithm proposed by Schmidl et al.

We refer to this region as the "*safe zone*" which can be seen in Fig. 4. The proposed method has a considerably lower probability of synchronization error in the places that BER is high and mainly has timing offsets in the *safe zone*. From $P_{error}(m)$ and $P_b(m)$, the average BER due to timing synchronization errors, $\bar{P}_b$, can be found: $\bar{P}_b = \sum_m P_b(m)P_{error}(m)$. $\bar{P}_b$ would be as follows for channel#1: $\bar{P}_{b,\text{method I}} = .398, \bar{P}_{b,\text{method II}} = .0079, \bar{P}_{b,\text{proposed method}} = 4.4 \times 10^{-4}$. Fig. 5 shows similar curves for channel#2. In this case, there will be more sensitivity to $m \leq -1$, since the delay spread spans 100% of the guard interval. This can be seen from P_b curves of Fig. 5, where there is no *safe zone*. This affects the shape of $P_{error}(m)$ of method III. It can be seen that the proposed synchronizer reduces the probability of timing errors at offsets that have high costs. However, method II still makes a considerable number of timing errors to the left which has a high cost for this channel. To see the effect of noise, Fig. 6 shows average bit error rate as a function of average received SNR for channel #1. The dashed line shows the BER of a perfect synchronizer for comparison. As can be seen, the performance of the proposed method is very close to that of the perfect synchronizer. The results confirm that the proposed algorithm is a robust timing synchronization method that works effectively even in considerably high delay spread fading environments, without requiring synchronization training information.

Next, we compare our proposed algorithm with some of the already existing ones in the literature. The method proposed in [17] is one of the most cited algorithms that use training information for synchronization. In their case, half of the subcarriers are occupied by known information for timing synchronization. Fig. 7 shows the performance of their algorithm for channel#1 and the aforementioned system parameters at $SNR = 20dB$. It can be seen that our proposed algorithm outperforms theirs considerably. Note that this is the case even though they transmit training information (and therefore known information) on half of the subcarriers, whereas we only use 25% of the subcarriers to send the pilot information. Therefore, with less waste of bandwidth, we achieved a considerably better performance.

Yang et al. [22] uses the pilots inserted for channel estimation to perform timing synchronization. However, they try to estimate the power-delay profile of the channel by averaging

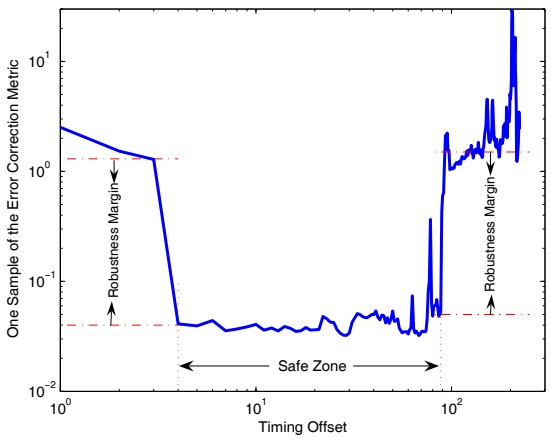

Fig. 8. Error correction metric as a function of the timing offset showing the robustness of the proposed method, our proposed method seeks to find the minimum of the metric.

over a number of OFDM symbols (around 10). Also they rely on the first path of the channel being the strongest, which may not be the case. In our case, we can correct for large timing offsets for channels that do not have the first power-delay profile path the strongest (see SFN channel of Fig. 3). Furthermore, we do the synchronization using only one OFDM symbol and without a need for averaging over a number of symbols.

Finally, Speth et al. [18] proposed using the redundancy of the cyclic prefix for coarse synchronization followed by fine tuning the performance by minimizing the following metric: $\sum_{l\in pilots}|z_l - p_l\tilde{H}(l)|^2$, as described in Section I. They provide a figure which represents their metric values as a function of the timing error (Fig. 7 of [18]). A more drastic change out of the *safe zone* is an indication of a better and more robust performance. In all their cases, the metric gets around 75% of its *safe zone* value even after 50 errors out of the safe zone. Fig. 8 shows a sample (note that this is one sample and not the average) of our metric function (MF of Section V) for comparison. In can be seen that the metric changes orders of magnitude immediately out of the safe zone, resulting in a considerably more robust timing synchronization, for a fading channel with even longer delay spread and more paths.

VII. Summary and Further Extensions

In this paper we proposed a robust timing synchronization algorithm for pilot-aided OFDM systems in low-mobility environments. We analytically characterized the impact of timing errors on the performance of pilot-aided channel estimation by deriving an expression for channel estimation error variance in the presence of timing errors and for a frequency-selective fading channel. The analysis showed that a pilot-aided channel esitmator is considerably sensitive to timing synchronization errors, due to the impact of rotations in different bases. We then showed how to utilize this sensitivity to design a robust timing synchronizer that requires no training information. The algorithm is a cross-block design that uses the sensitivity of the channel estimator to correct for timing synchronization errors. Simulation results confirmed mathematical derivations and showed the robust performance of the proposed algorithm in high delay spread fading environments. In part II of this paper, we show that the mathematical framework and the proposed algorithm can be extended for robust synchronization in high mobility cases and in the presence of a frequency offset.

References

[1] J. Bingham, "Multicarrier modulation for data transmission: An idea whose time has come," *IEEE Commun. Mag.*, vol. 28, no. 5, pp. 5-14, May 1990.

[2] H. Bolcskei, "Blind estimation of symbol timing and carrier frequency offset in wireless OFDM systems," *IEEE Trans. Commun.*, vol. 49, pp. 288-299, June 2001.

[3] B. Park, H. Cheon, C. Kang, and D. Hong, "A novel timing estimation method for OFDM systems," *IEEE Commun. Lett.*, vol. 7, no. 5, pp. 239-341, May 2003.

[4] L. Cimini, "Analysis and simulation of a digital mobile channel using orthogonal frequency division multiplexing," *IEEE Trans. Commun.*, vol. 33, pp. 665-675, July 1985.

[5] B. Le Floch, R. Hallbert-Lasalle, and D. Castellain, "Digital audio broadcasting to mobile receivers," *IEEE Trans. Consumer Electron.*, vol. 35, no. 3, pp. 493-503, Aug. 1989.

[6] M. Hsieh and C. Wei, "A low-complexity frame synchronization and frequency offset compensation scheme for OFDM systems over fading channels," *IEEE Trans. Veh. Technol.*, vol. 48, no. 5, Sep. 1999, pp. 1596-1609.

[7] William C. Jakes, *Microwave Mobile Communications*. New York: IEEE Press, 1974

[8] Y. Mostofi and D. Cox, "Mathematical analysis of the impact of timing synchronization errors on the performance of an OFDM system," *IEEE Trans. Commun.*, Feb. 2006.

[9] Y. Mostofi, "ICI mitigation and timing synchronization for pilot-aided OFDM mobile systems," Ph.D. thesis, Stanford University, Nov. 2003.

[10] H. Minn, V. K. Bhargava, and K. B. Letaief, "A robust timing and frequency synchronization for OFDM systems," *IEEE Trans. Wireless Commun.*, vol. 2, no. 4, July 2003, pp. 822-839.

[11] H. Minn, V. K. Bhargava, and K. B. Letaief, "A combined timing and frequency synchronization and channel estimation for OFDM," *IEEE Trans. Commun.*, vol. 54, no. 3, Mar. 2006, pp. 416-422

[12] S. Muller, "On the optimality of metrics for coarse frame synchronization in OFDM: A comparison," in *9th IEEE International Symposium PIMRC*, 1998, pp. 533-537.

[13] R. Negi and J. Cioffi, "Pilot tone selection for channel estimation in a mobile OFDM system," *IEEE Trans. Consumer Electron.*, vol. 44, no. 3, pp. 1122-1128, Aug. 1998.

[14] B. Park, H. Cheon; E. Ko, C. Kang, and D. Hong, "A blind OFDM synchronization algorithm based on cyclic correlation," *IEEE Signal Processing Lett.*, vol. 11, no. 2, pt. 1, pp. 83-85, Feb. 2004.

[15] Theodore S. Rappaport, *Wireless Communications: Principles and Practice*. Upper Saddle River, NJ: Prentice Hall, 1996

[16] H. Sari, G. Karam, and J. Janclaude, "Transmission techniques for digital TV broadcasting," *IEEE Commun. Mag.*, vol. 36, pp. 100-109, Feb. 1995

[17] T. M. Schmidl, "Synchronization algorithms for wireless data transmission using orthogonal frequency division multiplexing (OFDM)," Ph.D. dissertation, Stanford University, June 1997.

[18] M. Speth, F. Classen, and H. Meyr, "Frame synchronization of OFDM systems in frequency selective fading channels," in *Proc. IEEE 47th VTC*, 1997, pp. 1807-1811.

[19] J. Van de Beek, M. Sandell, and M. Isaksson, "Low-complex frame synchronization in OFDM systems," in *4th IEEE International Conf. Universal Pers. Commun.*, 1995, pp. 982-986.

[20] R. D.J. van Nee and R. Prasad, *OFDM for Wireless Multimedia Communications*. Boston, MA: Artech House, 1998.

[21] S. Weinstein and P. Ebert, "Data transmission by frequency-division multiplexing using the discrete Fourier transform," *IEEE Trans. Commun.*, vol. 19, pp. 628-634, Oct. 1971.

[22] B. Yang, K. Letaief and R. Cheng, "Timing recovery for OFDM transmission," *J. Select. Areas Commun.*, vol. 18, no. 11, Nov. 2000.

Yasamin Mostofi (S'98-M'04) received the B.S. degree in electrical engineering from Sharif University of Technology, Tehran, Iran, in 1997, and the M.S. and Ph.D. degrees from Stanford University, Stanford, CA, in 1999 and 2004, respectively. She is currently an assistant professor at the Department of Electrical and Computer Engineering at the University of New Mexico. Prior to that, she was a postdoctoral scholar at the California Institute of Technology from 2004 to 2006. Her research interests include cooperative sensor networks, mobile communications, control and dynamical systems and signal processing.

Donald C. Cox (S'58-M'61-SM'72-F'79) received the B.S. and M.S. degrees in Electrical Engineering from the University of Nebraska in 1959 and 1960, respectively, and the Ph.D. degree in Electrical Engineering from Stanford University in 1968. He received an Honorary Doctor of Science from the University of Nebraska in 1983.

From 1960 to 1963, Mr. Cox did microwave communications system design at Wright-Patterson AFB, Ohio. From 1963 to 1968 he was at Stanford University doing tunnel diode amplifier design and research on microwave propagation in the troposphere. From 1968 to 1973 his research at Bell Laboratories, Holmdel, New Jersey in mobile radio propagation and on high-capacity mobile radio systems provided important input to early cellular mobile radio system development, and is continuing to contribute to the evolution of digital cellular radio, wireless personal communications systems and cordless telephones. From 1973 to 1983 he was Supervisor of a group at Bell Laboratories that did innovative propagation and system research for millimeter-wave satellite communications. In 1978 he pioneered radio system and propagation research for low-power wireless personal communications systems. At Bell Laboratories in 1983 he organized and became Head of the Radio and Satellite Systems Research Department that became a Division in Bell Communications Research (Bellcore) with the breakup of the Bell System on January 1, 1984. He was Division Manager of that Radio Research Division until it again became a department in 1991. He continued as Executive Director of the Radio Research Department where he championed, led and contributed to research on all aspects of low-power wireless personal communications entitled Universal Digital Portable Communications (UDPC). He was instrumental in evolving the extensive research results into specifications that became the U.S. Standard for the Wireless or Personal Access Communications System (WACS or PACS). In September 1993 he became a Professor of Electrical Engineering and Director of the Center for Telecommunications at Stanford University where he continues to pursue research and teaching of wireless mobile and personal communications. He was appointed Harald Trap Friis Professor of Engineering in 1994.

Dr. Cox was a member of the Administrative Committee of the IEEE Antennas and Propagation Society (1986-88), was an Associate Editor of the IEEE TRANSACTIONS ON ANTENNAS AND PROPAGATION (1983-86), is a member of the National Academy of Engineering, is a member of Commissions B, C and F of USNC/URSI, and was a member of the URSI Intercommission Group on Time Domain Waveform Measurements (1982-84). He was awarded the IEEE 1993 Alexander Grapham Bell Medal "For pioneering and leadership in personal portable communications;" was a co-recipient of the 1983 International Marconi Prize in Electromagnetic Wave Propagation (Italy); received the IEEE 1985 Morris E. Leeds award and the IEEE Third Millennium Medal in 2000; and received the 1983 IEEE Vehicular Technology Society paper of the year award, and the IEEE Communications Society 1992 L. G. Abraham Prize Paper Award and 1990 Communications Magazine Prize Paper Award. He received the Bellcore Fellow Award in 1991. Dr. Cox is a fellow of AAAS and the Radio Club of America. He is author or coauthor of many papers and conference presentations, including many invited and several keynote addresses, and books. He has been granted 15 patents. Dr. Cox is a member of Sigma Xi, Sigma Tau, Eta Kappa Nu and Phi Mu Epsilon, and is a Registered Professional Engineer in Ohio and Nebraska.